



# Vertical Distributions of Suspended Sediment Concentrations in the Turbidity Maximum Zone of the Periodically and Partially Stratified Changjiang Estuary

Zhanhai Li<sup>1</sup> · Jianjun Jia<sup>1</sup> · Yongsheng Wu<sup>2</sup> · Haibo Zong<sup>1</sup> · Guoan Zhang<sup>1</sup> · Yax Ping Wang<sup>1</sup> · Yang Yang<sup>1</sup> · Liang Zhou<sup>1</sup> · Shu Gao<sup>1</sup>

Received: 5 May 2018 / Revised: 24 April 2019 / Accepted: 3 July 2019 / Published online: 16 July 2019  
© Coastal and Estuarine Research Federation 2019

## Abstract

The vertical distribution of suspended sediment concentration (SSC) plays a key role in the residual suspended sediment transport in the estuarine environments. A field measurement was carried out in the turbidity maximum zone (TMZ) of the Changjiang Estuary in 2012 to study the characteristics and formation mechanisms of SSC profile in the partially stratified estuary. Based on the observed data, we found that the vertical distribution of SSCs is mainly determined by the density stratification caused by the interactions between the river runoff and the saltwater intrusion. The vertical profiles of SSC were categorized into three types: (I) two-layer structure profile, (II) exponential profile, and (III) linear profile. Type I mainly occurred in condition of strong stratification, whereas types II and III mainly occurred in weak stratification and well-mixed conditions, respectively. We developed two new empirical equations to simulate the vertical profiles, which can accurately describe the observed exponential and linear profiles and reasonably/accurately describe the observed two-layer structure profiles. The two new equations can be easily used in other well-mixed or partially stratified estuaries given the surface and bottom SSC data, which can be obtained from many ways, for instance, the buoy and bottom tripod survey system, the remote-sensed images, and numerical models.

**Keywords** Vertical profile of suspended sediment concentration · Salinity · Density stratification · Bottom lateral current · Turbidity maximum zone · Partially stratified Changjiang Estuary

## Introduction

Transport of suspended sediment plays an important role in morphological changes and environmental pollution in estuarine and coastal waters (Dyer 1986; Uncles 2002; Shi 2010; Song et al. 2013). The transport flux is usually determined as a function of suspended sediment concentration (SSC), which usually has strong vertical distributions within the water column associated with several factors, such as sediment size,

cohesiveness, and turbulence intensity (e.g., Nielsen 1995; Shi et al. 1996; Ogston and Sternberg 2002).

Vertical distributions of SSC have been studied by many scientists through either field observations or laboratory flume experiments. In wave-controlled environments, for example, Nielsen (1995) noted that the horizontal convection of the water mass within the near-bottom layer played a key role in SSC profiles over a rippled bed, which was based on laboratory experiments. Using one diffusion-advection model, Lee et al. (2002) concluded that SSC profiles were dominated by both the vertical diffusion and vertical advection under storm and strong swell conditions. Ogston and Sternberg (2002) studied the effect of wave breaking on the SSC profiles and sediment flux profile in the surf zone. Wang (2012) investigated the SSC profiles under spilling and plunging breakers using a large-scale sediment transport facility and developed a combined breaking and turbulence length model. Due to weak sediment diffusivity and coarse bed sediment-induced low SSC levels, many field observations of SSC profiles in the wave environment are mainly focused on the near-bottom

---

Communicated by Paul A. Montagna,

✉ Zhanhai Li  
zhli@sklec.ecnu.edu.cn

<sup>1</sup> State Key Laboratory of Estuarine and Coastal Research, East China Normal University, Shanghai 200241, China

<sup>2</sup> Ocean Ecosystem Sciences Division, Fisheries and Oceans Canada, Bedford Institute of Oceanography, Dartmouth, Nova Scotia B2Y 4A2, Canada

water layer, which is generally within 0.5 m above the seabed (e.g., Vincent and Downing 1994; Sheng and Hay 1995).

The hydrodynamics and sediment dynamic conditions in estuarine environments are complicated and quite different from that in wave-controlled environments. In meso and macro-tidal estuaries, under the influence of tidal current and river flow, SSCs are relatively high and have different time scales of periodical and nonperiodic variations from seconds to years (e.g., Grabemann and Krause 2001; Wang et al. 2013; Li et al. 2015). In the partially and strongly stratified estuaries, strong density stratification can be yielded by saltwater intrusion and retreat processes, which can highly dampen the sediment diffusion coefficient and affect the vertical distribution of SSCs (Geyer 1993; Song and Wang 2013). In the Hudson River estuary, a stratification-modified Rouse equation was used to analyze the SSC profiles and suspended load (Orton and Kineke 2001). Field observations in the estuarine environment show that SSC profiles are complicated, which exhibits many different shapes and change remarkably with time. Based on several measured data sources, Liu et al. (2014) found that there are nine typical types of SSC profiles and many irregular shapes of SSC profiles in the inner and outer North Channel of the Changjiang Estuary. Using acoustic instruments, Shi et al. (1996) observed four typical types of SSC profiles with different formation mechanisms in the outer North Passage. Additionally, the time lags between suspended sediment transport and current velocity, which include erosion lag, scour lag, diffusion lag, and settling lag, may also exert important influences on the SSC profiles in the estuarine environment. This is due to the rapid changes in current velocity and SSC level, complex distribution of bed sediments, strong density stratification, and relative greater water depth (Dyer 1986; Wang 2002; Hoitink et al. 2003). At present, there are still many deficiencies in the understanding of the formation mechanisms of different SSC profiles types, and more field observations are needed. In the present study, we focus on the vertical distribution of a partially stratified estuary, the Changjiang Estuary.

The Changjiang Estuary is a world-famous estuary, which is characterized by a strong current velocity, high SSC level, and remarkable saltwater-freshwater mixing. This estuary is an ideal area in which to study the temporal variation and formation mechanism of SSC profiles in a partially stratified estuary. In situ observations were conducted in the turbidity maximum zone (TMZ) of the Changjiang Estuary in April 2012; the vertical profiles of SSC, current velocity and salinity were continuously measured from neap tide to spring tide for 16 tidal cycles. The observed SSC profiles displayed three typical types over a neap-spring tidal cycle and exhibited remarkable flood-ebb and neap-spring variation patterns. These patterns were highly affected by the hydrodynamic and

sediment dynamic conditions, including the factors of bottom lateral currents, salinity-induced stratification, and sediment resuspension and diffusion.

The purpose of this paper is to (1) display the types and temporal variation patterns of SSC profiles in a partially stratified estuary over the flood-ebb and neap-spring tidal cycles; (2) analyze the characteristics and formation mechanisms of different types of SSC profiles; and (3) predict the observed linear, exponential, and two-layer structure SSC profiles. .

## The Study Area

The Changjiang Estuary has three-order bifurcations and four outlets into the sea (Fig. 1). It is a semidiurnal, mesotidal, and hyposynchronous estuary, with the mean and maximum tidal ranges of 2.8 and 4.7 m, respectively. The tidal range decreases gradually from the river mouth to the upper reach because the friction exceeds the impact of convergence. The Changjiang Estuary is also a periodically partially stratified estuary (Shen et al. 2003; Song and Wang 2013), with salt wedge usually appeared in the neap tide. The water discharge of the Changjiang River is huge, with an annually mean of  $2.9 \times 10^4 \text{ m}^3/\text{s}$ , higher in wet season (May–October) while lower in dry season (November–April). The annual sediment discharge of the Changjiang River has reduced from 490 Mt/year (Mt, million tons) before the 1970s to 140 Mt/year in recent years, owing to the construction of numerous dams (in particular the Three Gorges Dam in 2003) and soil-conservation projects (Gao and Wang 2008; Yang et al. 2011; Yang et al. 2018). In recent 10 years, the annual mean amount of the sediment reduced to about  $1.4 \times 10^8$  tons. The magnitude and notable variability of the water and sediment discharges produce fundamental impacts on the hydrodynamics and morphological processes in the Changjiang Estuary

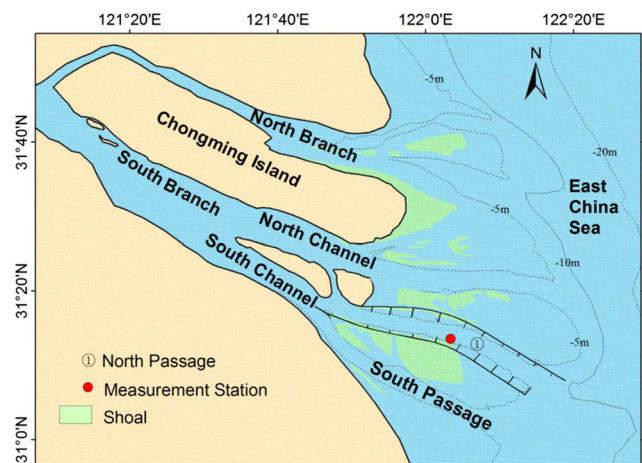


**Fig. 1** Measurement station in the North Passage of the Changjiang Estuary

and the adjacent waters, including the strength of current velocity, SSC level, saltwater intrusion, sediment transport flux, erosion, and siltation (Yang et al. 2011; Li et al. 2016).

The North Passage is an important channel in the Changjiang Estuary for riverine water and sediment transport to the sea, which is characterized by strong currents, high SSCs, and remarkable saltwater intrusion (Shen and Pan 2001; Wu et al. 2012). The TMZ develops in the North Passage, which is likely due to the combined effect of gravitational circulation and tide deformation (Shi and Chen 2000; Shi 2010). The observed maximum SSCs in the deep channel reached 20–40 g/l (Li et al. 2001; Shi et al. 2006; Wang 2016). The observed maximum surface current velocity reached 3.5 m/s, which appeared during the spring tides in the wet seasons. Gravitational circulation occurred in the North Passage during neap tides owing to the saltwater intrusion, which leads to density stratification and results in landward suspended sediment transport in the bottom water layer and seaward in the surface water layer (Pu et al. 2015; Wang 2016). Based on field observations, Song and Wang (2013) found that suspended sediment transport in the deep channel of the North Passage was strongly affected by the salinity distribution and salinity gradient-induced stratification. Additionally, construction of the Deepwater Channel Project has an obvious influence on the sediment dynamic process (Song et al. 2013). Suspended sediment in the North Passage is mainly composed of cohesive sediment particles; the mean grain size of the flocs generally ranged from 60 to 80  $\mu\text{m}$ , with a settling velocity of 0.1–0.3 cm/s (Shi and Zhou 2004). The median grain sizes of the bed sediments range from 6 to 101  $\mu\text{m}$ , with an average of 24  $\mu\text{m}$ . The predominant type of bed sediment is clayey silt.

## Materials and Methods

To explore the vertical distribution characteristics and temporal variation in the SSC profiles of the TMZ, field measurements were conducted at a fixed station in the North Passage during April 14–26, 2012, with typical neap and spring tides on April 14 and 26, respectively. The fixed survey station was located at the south shoal of the North Passage (Fig. 1), where the mean water depth is approximately 11 m, and the tidal range is 1.3–3.5 m. The axis of the main channel near the survey station is 280°. The current velocity and direction were measured using a shipboard acoustic Doppler current profiler (ADCP, 600 kHz), with a measurement interval of 30 s and vertical bin of 0.5 m. The vertical profiles of water turbidity, salinity, and water temperature were measured at the beginning of each hour using an optical backscatter sensor (OBS) with a measurement interval of 2 s. There were 204 SSC profiles obtained during the survey period. More than 500 l of water samples were collected during the neap, intermediate,

and spring tides. OBS calibration was conducted in the laboratory using the sediment that settled out of the water samples, and a high correlation existed between the turbidity and SSC data.

Both the salinity and SSCs displayed a strong temporal variation as well as a vertical variation during the survey period, which can generate strong density stratification and influence the SSC profiles by altering the sediment diffusion (Geyer 1993; Shi et al. 1996; Wang 2002). Following previous studies (Dyer 1986), the characteristics of density stratification induced by salinity and SSCs were evaluated by the gradient Richardson number ( $Ri$ ), which is as follows:

$$Ri = -\frac{g}{\rho} \frac{(\partial\rho/\partial z)}{(\partial u/\partial z)^2} \quad (1)$$

where  $g$  is the gravitational acceleration,  $\rho$  is the seawater density,  $u$  is the current velocity, and  $z$  is the vertical coordinate. The density stratification is negligible when  $Ri < 0.03$ , and the vertical mixing is completely suppressed when  $Ri > 0.25$  (Dyer 1986). The strength of the density stratification is determined by the competition between the vertical density gradient and velocity shear. To evaluate the relative importance of the salinity and suspended sediment to the stratification, we calculated the Richardson number based on the water density due to salinity and sediment concentration, respectively.

## Results

### Hydrodynamic Conditions During the Survey Period

#### Tidal Currents

The observed time series of the current velocity is shown in Fig. 2a, b. During the survey period, the tidal currents were strong in the North Passage, and the observed maximum current reached 260 cm/s. The tidally averaged current speeds ranged from 51 to 112 cm/s, which increased from neap tide to spring tide (Fig. 2a), and had a high positive linear relationship with the tidal ranges. The flood-ebb asymmetry in current velocity was significant in a tidal cycle (Fig. 2a). The ebb currents were remarkably larger than the flood currents, with the ratio between the currents reaching 1.5. The ebb current durations were also much longer than the flood current durations, which were 7.3 vs 5.1 h, respectively. The reversal of tidal current directions generally lagged behind the highest and lowest water levels for about 1.0 to 2.0 h. The mean Changjiang River discharge was  $2.2 \times 10^4 \text{ m}^3/\text{s}$  during the survey period. The strong river discharge was found to be the main reason for the flood-ebb current asymmetry in the

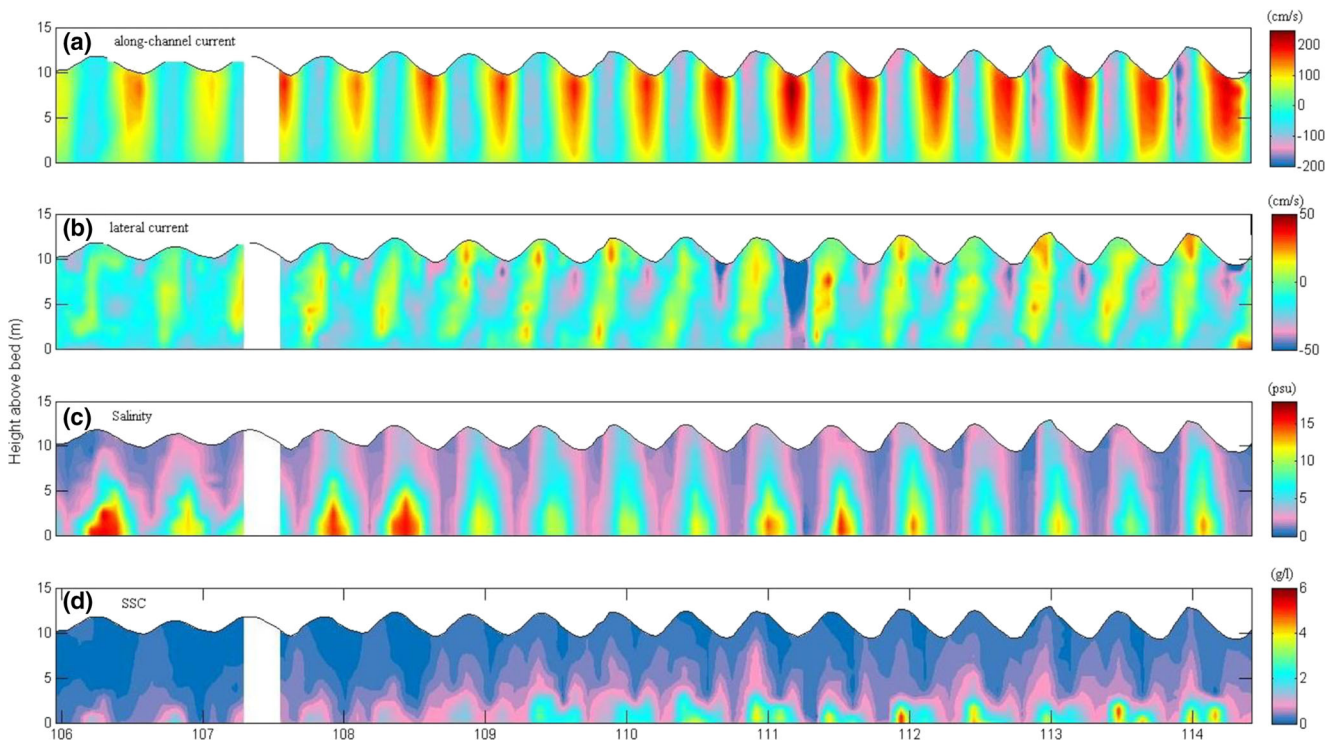


**Fig. 2** **a** Along-channel current velocity (positive seaward), **b** lateral current velocity (positive directed toward the north dike-side), **c** salinity, and **d** SSC from neap tide to spring tide. Note that the limit of the along-channel current is different from that of the lateral current

Changjiang Estuary because it largely enhanced the currents in the ebb and weakened the currents in the flood (Li et al. 2016).

The vertical profiles of current velocity displayed remarkable flood-ebb variation during the survey period. In flood phases, both the baroclinic and barotropic pressure directed landward, this caused the notable increase of near-bottom current velocity and the occurrence of vertical maximum current velocity in the middle or near-bottom water layers during the part of flood phases (Fig. 3a). But in ebb phases, the direction of baroclinic pressure was opposite to that of barotropic pressure, resulting in the notable decrease of near-bottom current

velocity and the occurrence of vertical maximum current velocity always in the surface water. As a consequence, the vertical gradient of current velocity in flood phase was much smaller than that in ebb phase (Fig. 3b).

As shown in Fig. 2b, the lateral currents were remarkable during the survey period. The bottom lateral currents directed toward the south flank during the ebb phases and the latter half of flood phases, about 80% of the total survey period. The strong lateral currents may be attributed to the dikes along the south side of the North Passage, which can exert important impact on the flow structure. Lateral circulation generally occurred during the latter half of flood phases in each tidal cycle,

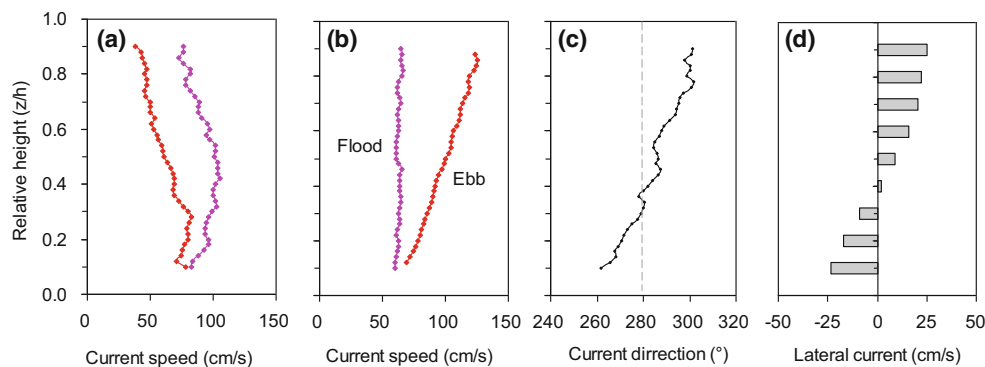


**Fig. 3** Examples of instantaneous current profiles during flood phase with max current appeared in the middle or bottom water layer (**a**), flood and ebb averaged current profiles (**b**), vertical profile of current direction in the middle and later flood phase when the lateral circulation

occurred (**c**), and vertical distribution of lateral current when lateral circulation occurred, with surface current directed to the north shoal and bottom current directed to the south shoal (**d**)

with the surface lateral currents directed toward the deep channel and the bottom lateral currents directed toward the south flank (Fig. 3c, d), and generally lasted for about 2 h. When the lateral circulation occurred, the maximum lateral current speeds could reach 20~30 cm/s during spring tides. The finding of lateral circulation is consistent with the previous model results of Song et al. (2013). The driving mechanism for the lateral circulation is not clear, but it is likely caused by the differential advection of salinity, which was found to be a major reason for the lateral circulation in estuaries (MacCready and Geyer 2010). This assumption was supported by previous studies (e.g., Shen and Pan 2001; Shen et al. 2003), which concluded that saltwater intrusion was stronger in the deep channel than in the shoal in the North Passage.

16.0 psu/m, with a mean value of 4.0; the salinity gradient ranged from 0.0 to 1.3 psu/m, with a mean value of 0.4 psu/m.

The tidally averaged salinity ranged from 3.0 to 5.0 psu, which slowly increased from neap tide to spring tide. During the neap tide, due to the weak current velocity, the vertical mixing of salinity was weak, and the salt wedge appeared during the flood phase and early half of the ebb phase. However, during spring tide, the salt wedge disappeared due to the strong spring currents. Especially during the early half of the flood phase and latter half of the ebb phase, the salinity reduced to a very low level and was well-mixed in the entire water column. Consequently, the salinity-induced pycnocline was notable during the neap tide, yet it rarely appeared during the spring tide.

### Salinity

The temporal variations of salinity are shown in Fig. 2c, which reflect the North Passage is highly affected by the saltwater intrusion and retreat processes. In a tidal cycle, both the salinity and its vertical gradient displayed remarkable flood-ebb variation patterns. To provide more detail on the salinity in a tidal cycle, we plotted an example of the salinity distribution during a tidal cycle in Fig. 4. The salinity increases with the development of the flood, and simultaneously, the stratification becomes stronger (Fig. 4a). In contrast, the salinity decreases in the ebb, and the stratification gradually weakens with time (Fig. 4b). The maximum salinity and salinity gradient always appeared during the high-water slack period, and the minimum values always appeared in the low-water slack period. Over the survey period, the salinity ranged from 0.5 to

### Density Stratification

Salinity produced strong density stratification during the survey period (Fig. 5a). Sixty-five percent of the  $Ri$  were significantly larger than the critical value of 0.25, indicating that the vertical mixing of suspended sediment was completely damped and the profile of SSC was highly affected in these periods.  $Ri$  was generally less than 0.25 during the early flood and middle to later ebb in the spring and intermediate tides due to the smaller vertical salinity gradient, implying the impact of the salinity-induced stratification on the vertical mixing of suspended sediment was remarkably reduced during these periods. In a tidal cycle, the density stratification was usually greater in the flood phases than the ebb phases, mainly because the vertical current gradients were much smaller during the flood than during the ebb (Fig. 3b). Resulting from the

**Fig. 4** Example of the salinity profile variation pattern during the flood and ebb phases (in the fifth tidal cycle), hour  $n$  denotes the  $n$ th hour during the flood and ebb phases

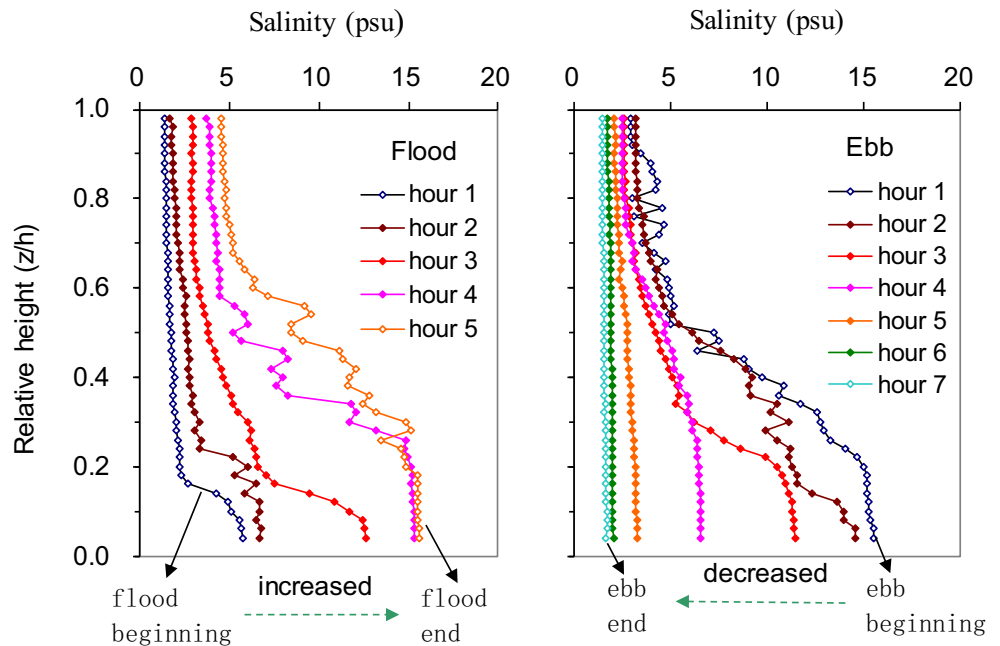
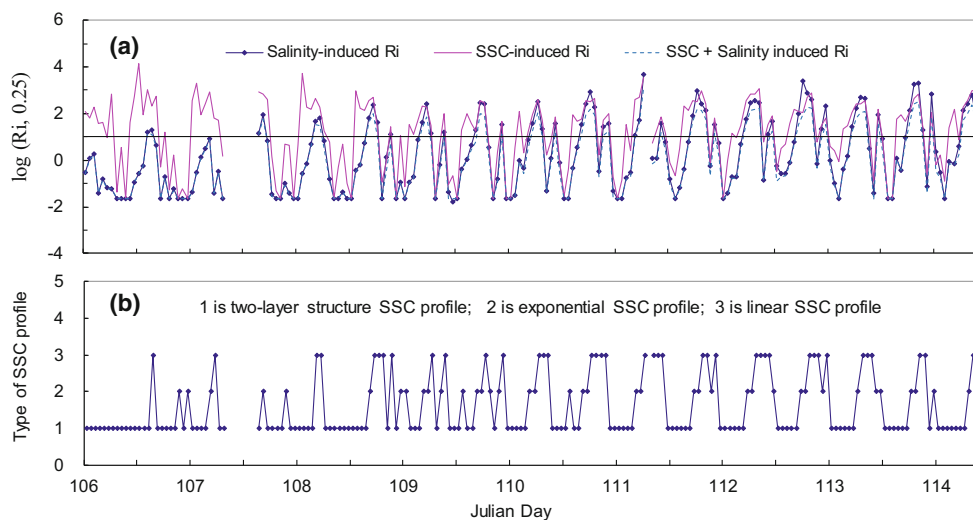


**Fig. 5** Time series of the gradient Richardson number calculated according to the data measured at the 0.15 and 0.85 h water layers (a) and type of SSC profiles (b) during the survey period



combination of larger salinity gradient and smaller current gradient, the density stratification was strong from the middle flood to the middle ebb, and the tidal maximum stratification usually appeared during the high-water slack period.

From the neap tide to the intermediate and spring tides, the salinity-induced stratification gradually decreased. For example, the occurrence of  $Ri > 0.25$  in the 1st, 8th, and 15th tidal cycles was 100, 67, and 58%, respectively, which indicates that the vertical mixing of SSC was enhanced from neap tide to spring tide with the increase of current velocity, and the impact of salinity-induced stratification on the SSC profiles would be gradually decreased. Song and Wang (2013) also revealed that the density stratification was stronger during the neap tide than during the spring tide in the North Passage, which is consistent with our finding.

As shown in Fig. 5a, the SSC could also produce strong density stratification. During the survey period, 45% of the SSC-induced gradient Richardson number was significantly larger than the critical value of 0.25, which occurred mainly during the flood phases and early ebb phases owing to the combination of the larger SSC gradient and smaller current gradient. During a tidal cycle, the SSC-induced stratification was remarkably stronger during the flood phase than the ebb phase, which is similar to the variation pattern of salinity-induced stratification.

A comparison showed that during 85% of the survey period, the salinity-induced stratification was significantly larger than the SSC-induced stratification, which demonstrates that the influence of salinity on the damping of sediment diffusion and SSC profile was clearly stronger than that of the SSC. Previous studies show that sediment contribution to the water density of 1 g/l equals salinity increase of 0.76 psu (Fohrmann et al. 1998; Wang and Wang 2010), which also indicates that SSC gradient contribution to the density stratification of 1 g/l/m equals salinity gradient increase of 0.76 psu/m. During the survey period, the averaged SSC gradient was 0.12 g/l/m, only

equivalent to a salinity gradient of 0.09 psu/m ( $= 0.12 \times 0.76$ ), whereas the averaged salinity gradient was as high as 0.42 psu/m. This is the major reason why the salinity-induced stratification was much larger than the SSC-induced stratification.

Density stratification induced by the combination of salinity and SSC was further enhanced during the survey period (Fig. 5a). Seventy percent of the calculated gradient Richardson numbers were larger than 0.25, which is higher than the salinity or solely SSC-induced stratification. The variation pattern of the combined stratification was similar to the salinity-induced stratification because the salinity-induced stratification was much stronger than the SSC-induced stratification.

In brief, both the salinity and SSC could produce strong density stratification in the North Passage. The density stratification was stronger during the spring tide than during the neap tide and during the flood phases than during the ebb phases. During 70% of the survey period, sediment diffusion was highly dampened by the strong density stratification.

## Temporal Variation of SSC Profiles

### The General Characteristic of SSC

The North Passage is located at the TMZ of the Changjiang Estuary. The SSCs are relatively high and have remarkable neap-spring and flood-ebb variations (Fig. 2d). During the survey period, the tidally averaged SSCs ranged from 0.19 to 0.96 g/l, and the observed maximum value reached 6.07 g/l. Affected by the increase in tidal currents, the SSCs increased from neap tide to spring tide, with a ratio of 4.5 between the spring and neap tides. During most tidal cycles, the averaged SSCs in the flood phases were greater than those in the ebb phases, with a ratio of 1.1 between them. The

maximum SSC during a tidal cycle generally appeared in the flood phase.

On the subtidal time scale, the tidal mean SSCs had a high positive linear relationship with the tidal mean currents over the survey period (Fig. 6a). Such relationship was also observed in other channels of the Changjiang Estuary (Li et al. 2015; Li et al. 2016), indicating that the tidal mean SSCs were highly modulated by tide. Whereas, the correlation was complicated between the bottom SSC and depth mean current velocity on the intratidal time scale. A typical example is shown in Fig. 6b. It displayed that the bottom SSCs increased with the increase of current velocity in the first 2 h of flood phase. But during the following 2 h, bottom SSCs sharply increased with the decrease of current velocity. At the 4th hour of this flood, the bottom SSC was as high as 5.5 g/l, whereas the mean velocity was only 50 cm/s. During the 2 h, the bottom lateral currents were stronger and directed toward the south flank of this channel. During the ebb phase, the bottom SSCs increased with the increase of ebb currents until the peak period, then decreased gradually with the decrease of ebb currents.

### Types of SSC Profile

During the survey period, 204 SSC profiles were obtained from neap tide to spring tide in the TMZ of the North Passage, which displayed obvious intratidal and neap-spring variations. Based on the overall shape of the SSC curve within the entire water column, the observed SSC profiles were summarized into three types. As shown in Fig. 7, the three typical

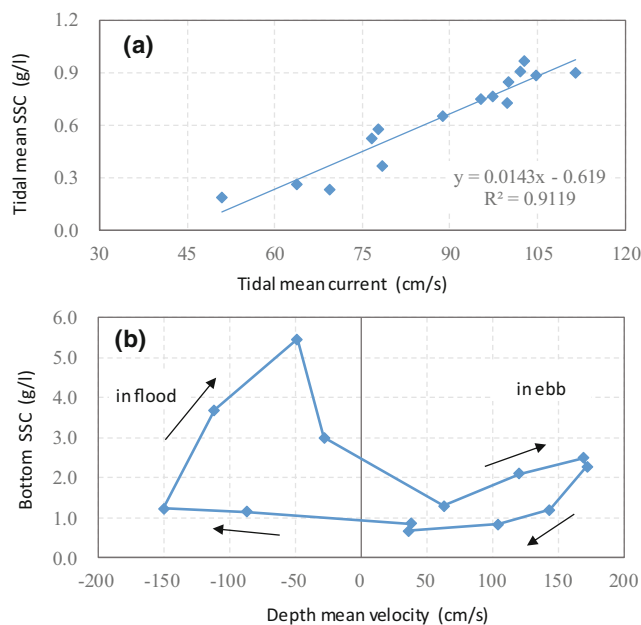


**Fig. 6** Correlation between tidal mean SSC and tidal mean current during the neap-spring tidal cycle (a); example of the correlation between instantaneous bottom SSC at 0.05 h and depth mean velocity in the 15th tidal cycle (b)

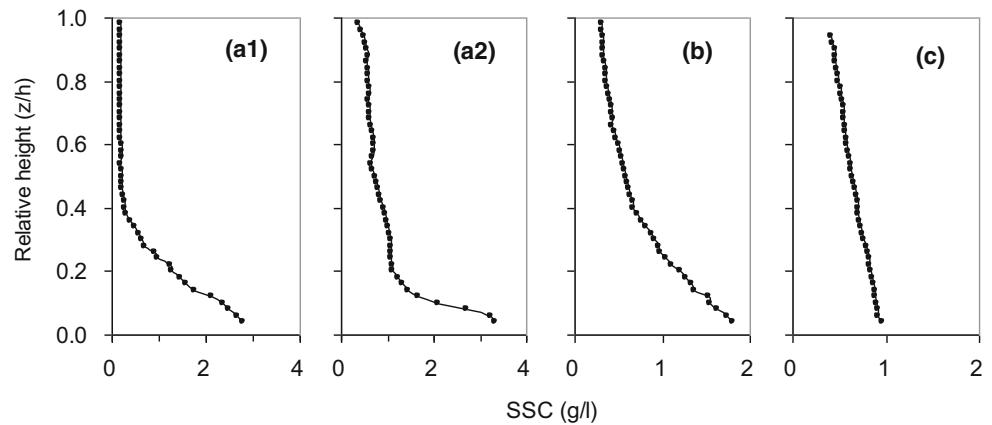
types are the two-layer structure profile, exponential profile, and linear profile. There are two major reasons for us to classify the observed SSC profiles: (1) owing to the complicated vertical distribution and temporal variation in the SSC profiles, classification can help us conveniently delineate the structure of the SSC profiles, and (2) different types of SSC profiles should have different shapes, formation mechanisms, and controlling factors, and thus, classification can help us to clearly analyze the mechanisms of different SSC profile types. The time series of the types of SSC profiles during the survey period are displayed in Fig. 5b.

The typical shapes of the two-layer structure SSC profiles are shown in Fig. 7a, which was characterized by higher SSCs appearing in the lower water column and lower SSCs appearing in the upper water column. The difference in the SSC level between the lower and upper layers was significant. The vertical gradient of SSCs in the lower layer was strikingly larger than that in the upper layer, and a remarkable pycnocline existed between the lower and upper layers. This kind of SSC profile had a high occurrence frequency during the survey period, which accounted for 60% of the total profiles. Influenced by the weak tidal currents and vertical mixing, most of the observed SSC profiles in the neap tides were the two-layer structure profile (Fig. 5b). During the spring and intermediate tides, this kind of profile mainly appeared during the latter half of the flood and early half of the ebb with large salinity gradient and weak current velocity.

The shape of the exponential SSC profile is shown in Fig. 7b, which is characterized by SSCs increasing exponentially from the surface layer to the bottom layer, with a relatively smaller ratio between the bottom and surface SSCs. Meanwhile, the vertical gradients of SSCs also increased from the surface to the bottom, and the curve of the profile was continuous in the water column; i.e., there was no remarkable pycnocline or sudden change in the SSC profile. During the survey period, approximately 20% of the observed profiles were exponential profiles. Most of the exponential profiles appeared during the ebb peak current period, which generally lasted 1 h. Sometimes, the exponential profile also appeared during the first 1–2 h of the flood phases during the spring and intermediate tides. When the exponential profile occurred, the current velocity was strong, the salinity gradient was small, and the  $Ri$  was generally less than the critical value of 0.25 (Fig. 5b). Weak stratification should be one of the basic prerequisites for the formation of this kind of profile.

The shape of the linear SSC profile is shown in Fig. 7c, which is characterized by SSCs increasing linearly from the surface layer to the bottom layer, with a constant SSC gradient in the entire water column and small ratio between the bottom and surface SSCs. Linear profiles mainly appeared in the later ebb phase with the decrease of current velocity, which generally lasted for approximately 1–2 h, and also appeared in the early flood phases. The occurrence of this kind of profile was

**Fig. 7** Three typical types of SSC profiles are observed during the survey period: **a1** and **a2** are the two-layer structure SSC profile, and **b** and **c** are the exponential and linear SSC profiles, respectively



20% during the survey period, which is close to the exponential profile but lower than the two-layer structure profile. When the linear profiles appeared, the salinity was very low and well-mixed in the water column, and the density stratification was weak.

Statistical results show that there are obvious differences in hydrodynamic and sediment dynamics for these three types of SSC profiles, which implies the differences in their characteristics and formation mechanisms. As shown in Table 1, the two-layer profile occurred during the weak current speed, large salinity, and strong stratification period, and characterized by large SSC gradient. Whereas, the exponential and linear profiles occurred during the strong current speed, small salinity, and weak stratification period, with small SSC gradient. The formation mechanism of the two-layer structure profile was mainly attributed to the strong bottom lateral currents and associated density stratification during the survey period. The bottom lateral currents, which directed toward the south flank, could transport the high-SSC and high-salinity water from the deep channel to the south shoal, and the strong stratification damped the near-bottom high SSC to diffuse into the middle and upper water layers. Previous studies have also shown that strong stratification is an important reason for the formation of the two-layer structure profile (e.g., Geyer 1993; Wang 2012). In addition, the current-induced resuspension and advection may play a minor role for the formation of the

two-layer structure profile. The discontinuity of the curve of the two-layer structure profile means that the vertical distribution of SSCs did not reach the equilibrium state in the whole water column. The exponential and linear profiles mainly occurred during the ebb peak and flood peak period and the latter half of ebb phase. Due to the strong current velocity and the long mixing time, the suspended sediment was fully mixed in the whole water column. The continuity of the exponential and linear profiles means that the vertical distribution of SSCs approached the equilibrium state in the whole water column.

The type of the linear SSC profile was not observed in the outer Changjiang Estuary by Shi et al. (1996), and the reason may be attributed to the small current velocity, weak vertical mixing, and relatively large water depth in the survey area. The type of jet-shaped profile was observed by Shi et al. (1996) during the peak flood and peak ebb periods, which resulted from strong entrainment of SSC and small settling velocity, and this kind profile was not observed during our survey period. In the inner and outer North Channel of the Changjiang Estuary, nine typical types of SSC profiles, including the two-layer structure profile, exponential profile, and linear profile, were observed by Liu et al. (2014). Additionally, Liu et al. (2014) also observed many irregular-shaped SSC profiles, which accounted for approximately 45% of the total SSC profiles. The appearance of so many types and

**Table 1** Characteristic values of current velocity, salinity, and SSC during the occurrence of different SSC profile types

Types of SSC profile	Averaged current velocity (cm/s)	Averaged salinity (psu)	Averaged salinity gradient (psu/m)	Difference between bottom and surface salinity (psu)	Averaged SSC (g/l)	Averaged SSC gradient (g/l/m)	Difference between bottom and surface SSCs (g/l)	Averaged SSC inventory (kg/m <sup>2</sup> )
Two-layer structure profile	72	5.0	0.6	6.4	0.5	0.14	1.6	6.1
Exponential profile	122	3.1	0.3	2.8	0.6	0.10	1.1	5.9
Linear profile	90	1.7	0.1	0.7	0.5	0.04	0.4	5.0

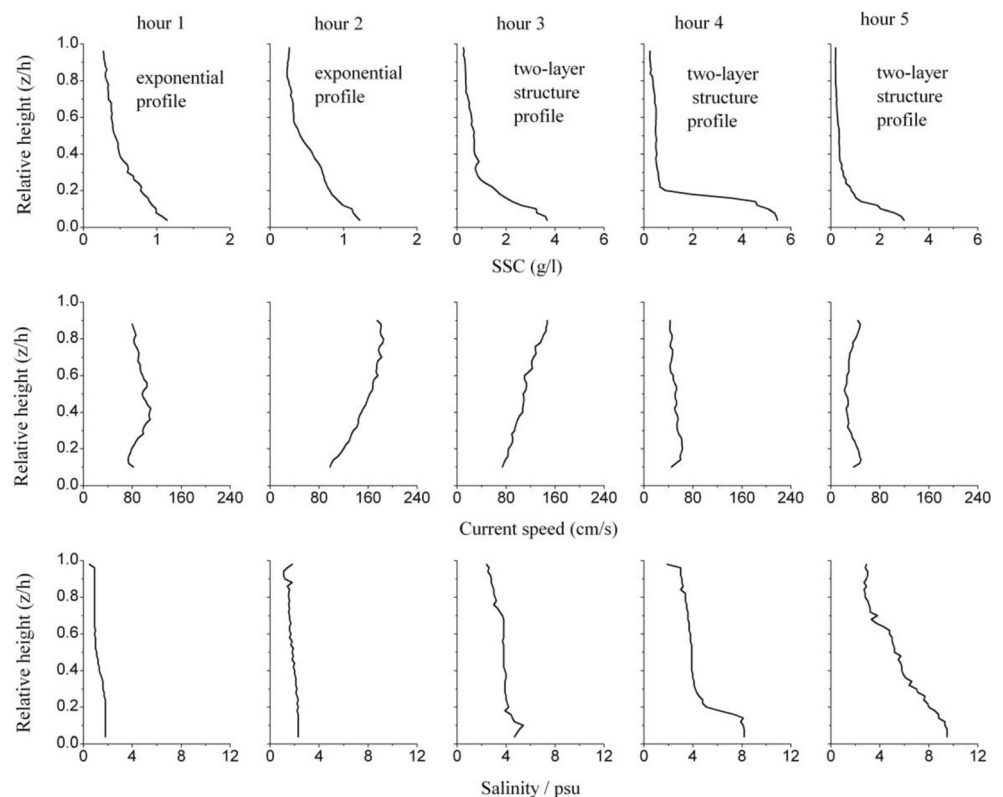
irregular shapes of SSC profiles might be related to the complex hydrodynamics and sediment dynamics condition in the North Channel, including rotary currents, vertical variations in current direction, intensive saltwater intrusion, strong density stratification, and complex spatial distribution of bed sediments.

### Flood-Ebb and Neap-Spring Variation Patterns of SSC Profile

The temporal variation in the SSC profiles during spring and intermediate tides displayed remarkable flood-ebb patterns. The 15th tidal cycle was used as an example to delineate such variation. As shown in Fig. 8, the flood phase generally lasted for about 5 h, and the peak currents generally occurred at the second or third hour. During the first 2 h, SSCs were enhanced with the increase of current velocity. In response to the very small salinity gradient and its associated weak density stratification during this period, many SSC profiles were exponential and/or linear profiles. During the last 3 h of the flood phase, with the remarkable decrease of the current velocity, the near-bottom SSCs abruptly increased (Fig. 8), yet the surface SSCs still remained at a very low level and was very close to the preceding value. As a result, the two-layer structure profiles were yielded, and this kind of profile occurred stably during the middle and later flood phases over the survey period.

The ebb phase generally lasted for 7 h during the spring and intermediate tides. The occurrence of the SSC profile during the ebb phase was on the order of a two-layer structure profile, exponential profile, and linear profile (Fig. 9). Accompanied by the larger salinity gradient and strong density stratification, SSC profiles during the first 3 h were the two-layer structure profile, with a notably higher SSC in the near-bottom water layer caused by the lateral currents and resuspension of bed sediments, and a very low SSC in the upper water layer. A significant pycnocline existed between the upper and lower layers in these SSC profiles. At the 4th hour, the ebb currents generally reached the peak value, and the SSC profile was in a transitional state; i.e., sometimes it was the two-layer structure profile, and sometimes it was the exponential profile. With the strong current velocity and very small salinity gradients at the 5th hour, SSC profiles were the exponential profiles. In the final 2 h of the ebb phase, the current velocity further decreased, and the salinity was in a well-mixed condition, the SSC profiles under such hydrodynamic conditions were mainly the linear profiles. Suspended sediments were generally diffused to the water surface near the middle of the ebb phases during the intermediate and spring tides, and this phenomenon was also observed by the authors in the South Passage of the Changjiang Estuary. In brief, modulated by the variation of current velocity, salinity gradient, and density stratification, the SSC profiles evolved from one type to another during the ebb phase, i.e., from the

**Fig. 8** Temporal variations in the SSC profile, current profile, and salinity profile during the flood phase of the 15th tidal cycle; hour  $n$  denotes the  $n$ th hour during the flood



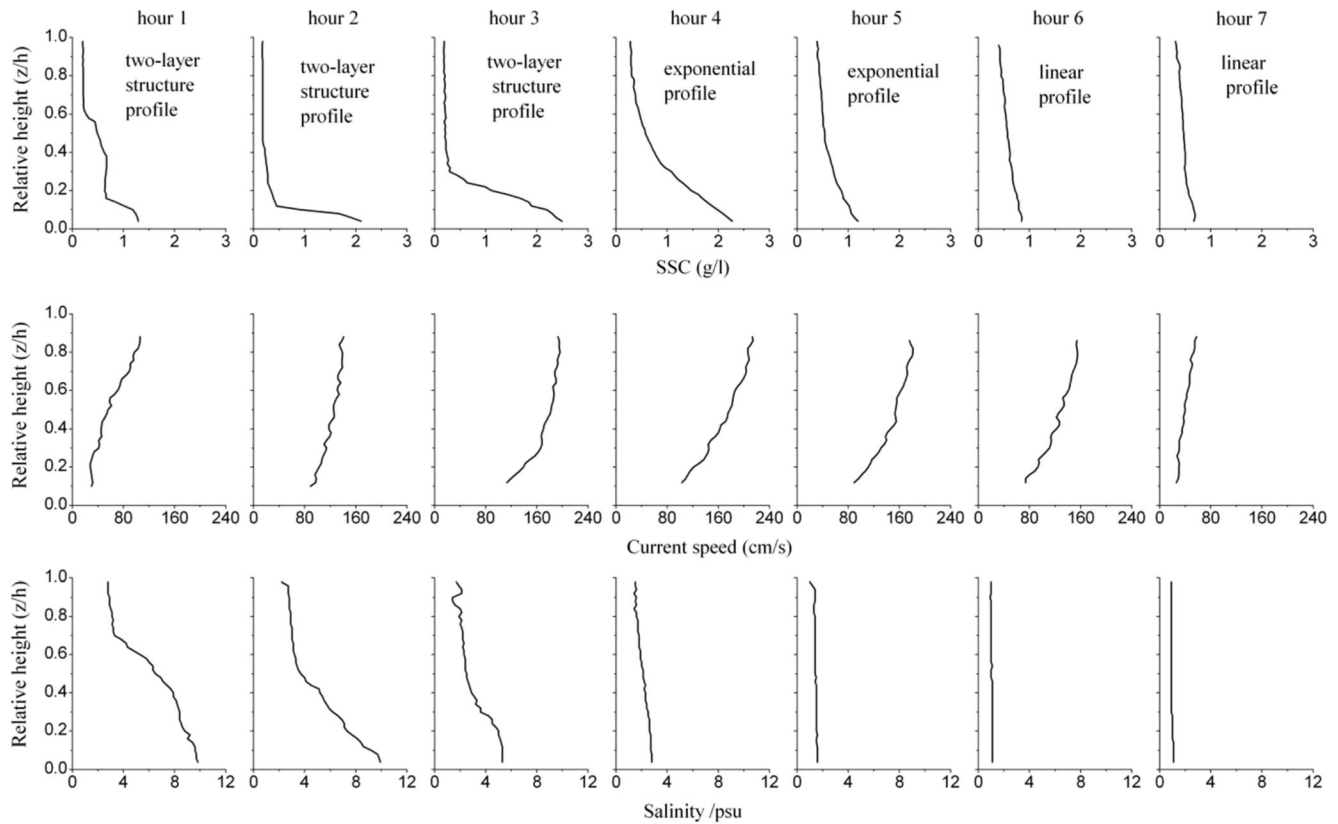


**Fig. 9** Temporal variations in the SSC profile, current profile, and salinity profile during the ebb phase of the 15th tidal cycle; hour  $n$  denotes the  $n$ th hour during the ebb phase

two-layer structure profile to the exponential profile and further to the linear profile.

The neap-spring variation in the SSC profiles was significant. During the neap tides, most of the SSC profiles were two-layer structure profiles due to the weak current velocity and salinity-induced strong density stratification. During spring tides, in addition to the occurrence of the two-layer structure profile during the strong stratification period, exponential and linear profiles also occurred. The variations in the SSC profiles during the intermediate tides were the transitions of the spring tide and neap tide. Generally, with the increase of current velocity and decrease of density stratification, the occurrence of the two-layer structure profile was reduced and the occurrence of the exponential and linear profiles increased from neap tide to spring tide.

### Empirical Equations for Different Types of SSC Profile

Accurate prediction of the vertical distribution of SSCs is a critical scientific issue in estuarine sediment dynamic research. Soulsby (2000) proposed an empirical equation to predict the linear SSC profile using the near surface and near bed SSCs, and the expression of the equation is as follows:

$$\frac{C_z}{C_b} = -\frac{R-1}{R} \cdot \frac{z}{h} \quad (2)$$

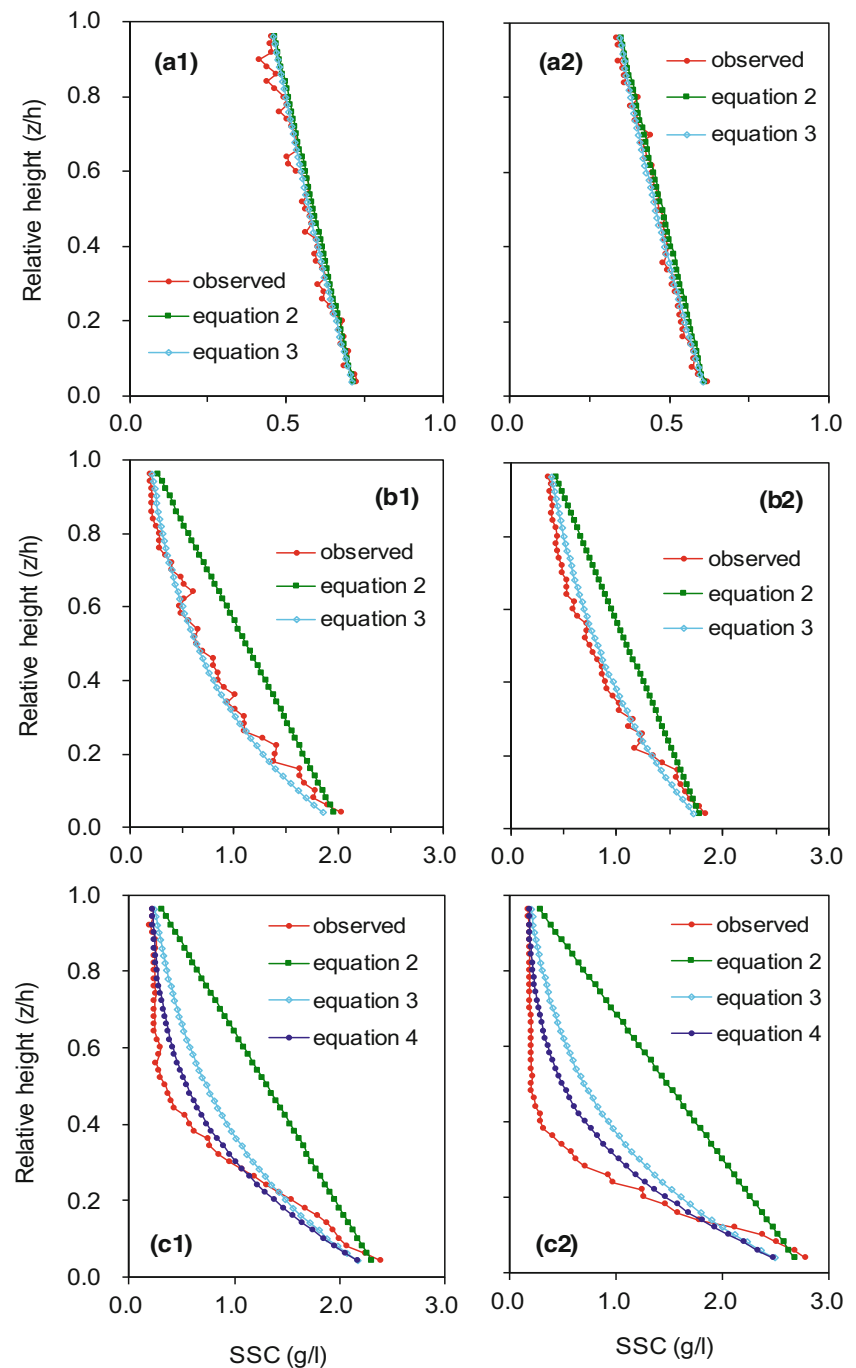
$C_z$  is the SSC at height  $z$  above the bed,  $C_b$  is the SSC near the bed,  $R$  is the ratio of the near surface SSC to the near bed SSC, and  $h$  is the water depth. During the survey period, the observed linear profiles, which accounted for 20% of the total profiles, agreed very well with Eq. 2. As shown in Fig. 10a, the SSC profiles predicted by Eq. 2 were very close to the observed linear profiles.

A larger error existed between the observed and predicted exponential profiles by Eq. 2. As shown in Fig. 10b, the mean error between the predicted and observed profiles was 37 and 28%, respectively, which was calculated by (the mean predicted SSC – the mean observed SSC)/the mean observed SSC. In order to improve the prediction accuracy of the exponential profile, Eq. 2 should be modified. The analysis showed that there existed a very good linear relationship between  $z - \ln(\text{SSC})$  for each observed exponential profile, with the correlation coefficient generally larger than 0.95. Based on the linear relationship between  $z - \ln(\text{SSC})$ , Eq. 2 was modified into the following form:

$$\frac{\ln C_z}{\ln C_b} = 1 - \frac{R_m - 1}{R_m} \cdot \frac{z}{h} \quad (3)$$

where  $R_m$  is the ratio of  $\ln C_s$  to  $\ln C_b$ , and  $C_s$  is the SSC near the water surface. During the survey period, the

**Fig. 10** Comparison of observed linear (**a1**, **a2**), exponential (**b1**, **b2**), and two-layer structure (**c1**, **c2**) SSC profiles with their predicted SSC profiles using Eqs. 2, 3, and 4



observed exponential profiles, which accounted for approximately 20% of the total SSC profiles, were fitted very well to Eq. 3. As shown in Fig. 10b, the SSC profiles predicted with Eq. 3 were very close to the observed exponential profiles, with prediction errors of only  $-6$  and  $4\%$ , respectively. This demonstrates that Eq. 3 can accurately predict the exponential SSC profile.

There was also a very good linear relationship between  $z - \ln(\text{SSC})$  for each observed linear profile, with the correlation coefficient sometimes reaching 0.99. Based on such

feature, the linear profile can be treated as a special type of exponential profile. To evaluate this point, Eq. 3 was used to predict the linear SSC profile. As shown in Fig. 10a, the SSC profiles predicted with Eq. 3 were very close to the observed linear profiles, with the prediction accuracy being almost the same as that obtained with Eq. 2, demonstrating that both the exponential and linear profiles can be accurately predicted with Eq. 3. During the survey period, approximately 40% of the total profiles (both the linear and exponential profiles) were fitted to Eq. 3.

The observed two-layer structure profile was generally concave upward, and to some extent, the two-layer structure profile was similar to the shape of the exponential profile. Equations 2 and 3 were tested to predict the two-layer structure profile. Figure 10c revealed that Eq. 2 was not suitable for predicting the two-layer structure profile because of a large error. The prediction accuracy of Eq. 3 was much better than that of Eq. 2, but notable error still existed (Fig. 10c). To improve the prediction accuracy, Eq. 3 was further modified into the following form:

$$\frac{\ln C_z}{\ln C_b} = 1 - \frac{R_m - 1}{R_m} \cdot \frac{z}{h} \cdot \left( 1 + \frac{z}{h} \left( 1 - \frac{z}{h} \right) \right) \quad (4)$$

As shown in Fig. 10c, the prediction accuracy of Eq. 4 was obviously higher than that of Eqs. 3 and 2. The mean prediction error of Eq. 4 in Fig. 10c was only 4 and 20%, respectively, which indicates that Eq. 4 could predict the two-layer structure profile accurately and reasonably. Generally speaking, the prediction accuracy of Eq. 4 will be greater when the ratio between the bottom and surface SSCs is relative small.

During the survey period, many two-layer structure SSC profiles can be treated as the combination of the two exponential profiles, i.e., the upper and lower exponential profiles (Figs. 8, 9, and 10c), and the vertical distribution of these profiles can also be predicted accurately or reasonably by this method. For example, the mean prediction error for the SSC profiles at the hours 3 and 5 in Fig. 8 was only –5 and 6% respectively, and was 15 and –16% for the SSC profiles at the hours 2 and 3 in Fig. 9. Therefore, it is an alternative method for predicting the two-layer structure SSC profiles.

With the development of the field observation technique, the surface and bottom SSCs can be accurately and continuously measured for long-term periods using the buoy and bottom tripod survey system. Under such situations, Eqs. 3 and 4 can be used to predict the vertical distribution of SSCs. The previously observed exponential, linear, and two-layer structure profiles by Liu et al. (2014) and Shi et al. (1996) should fit Eqs. 3 and 4. Additionally, the SSC profiles with constant SSC values within the entire water column were observed by the authors during the later ebb phase of the spring tides in the South Passage of the Changjiang Estuary, which can also be predicted accurately by Eq. 3.

Some theoretical and empirical equations have been proposed to describe and predict the different types of SSC profiles (e.g., Dyer 1986; Nielsen 1995; Soulsby 1997; Whitehouse et al. 2000; Van Rijn 2007), but many of them contain several important parameters, including the reference sediment concentration, settling velocity, diffusion coefficient, and shear velocity. In complex estuarine and coastal environments, measuring and obtaining suitable values for these parameters is difficult, which seriously affects the

prediction accuracy of these equations and their applications in real environments. In comparison, Eqs. 3 and 4 are simple, reliable, and easy to use because they only contain three easily obtained parameters, i.e., the near surface and near bed SSCs and the water depth.

## Sediment Diffusivity Coefficients of the Exponential and Linear SSC Profiles

Sediment eddy diffusivity is a key parameter for the vertical distribution of SSCs. Previous studies showed that the vertical distribution of sediment eddy diffusivity is complicated, and has several patterns, including linear, parabolic, two-layer and three-layer structures, and constant distribution (e.g., Sheng and Hay 1995; Whitehouse et al. 2000; Lee et al. 2002; Van Rijn 2007; Thorne et al. 2009; Wang 2012). An important question is as follows: what is the major characteristic of sediment diffusivity in the North Passage of the Changjiang Estuary? Sediment diffusivity of the exponential and linear profiles will be analyzed in this study. Owing to the complicated shape and vertical variation in the SSC gradient, the sediment diffusivity of the two-layer structure profile will be studied in the future.

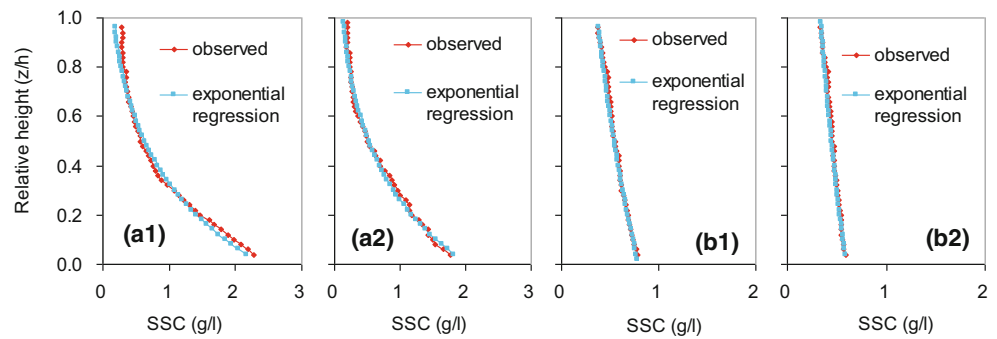
Previous studies revealed that the following equation is established when the sediment diffusion flux equals the settling flux (Dyer 1986):

$$Ws \cdot C = \varepsilon \cdot \frac{dc}{dz} \quad (5)$$

where  $Ws$  is the settling velocity,  $\varepsilon$  is the sediment diffusivity coefficient, and  $C$  is the SSC.  $\varepsilon$  and its vertical distribution can be derived based on Eq. 5 when the SSC profile is known. In the Changjiang Estuary TMZ, suspended sediments are mainly composed of fine cohesive sediments, and the settling velocity of the flocs mainly ranged from 0.1 to 0.3 cm/s (Shi and Zhou 2004). According to the settling velocity range, we use the median value of 0.2 cm/s as the settling velocity of suspended sediment in the North Passage. A similar settling velocity of 0.22 cm/s has been used to predict the SSC profile in the Hudson River (Orton and Kineke 2001).

To explore the magnitude and vertical distribution of the sediment diffusivity coefficient, the observed exponential profile was first transformed into the standard exponential profile through exponential fitting. As shown in Fig. 11(a1, a2), the fitted standard exponential profiles were very close to the observed profiles, indicating that the former could reflect the major characteristic of the latter. The diffusivity coefficients were calculated according to Eq. 5 and the fitted standard profile. The results showed that the diffusivity coefficient of the exponential profile was a constant value within the entire

**Fig. 11** Comparison of observed exponential (a1, a2) and linear (b1, b2) SSC profiles with their exponential regression lines



water column, which ranged from 0.006 to 0.026 m<sup>2</sup>/s during the survey period, with the mean value of 0.013 m<sup>2</sup>/s.

For the exponential profile, the following relationship exists:

$$\frac{C_{z+\Delta z}}{C_z} = \frac{C_{z+2\Delta z}}{C_{z+\Delta z}} = \frac{C_{z+3\Delta z}}{C_{z+2\Delta z}} = \Lambda = \frac{C_{z+H\Delta z}}{C_{z+(H-1)\Delta z}} = \text{constant} \quad (6)$$

which means that for a fixed water interval, the ratio of SSCs between the adjacent water layers is a constant value, that is, the SSCs decrease from the bottom layer to the surface layer at a fixed ratio. For example, for the exponential profile that appeared at the 5th hour of the ebb phase in the 15th tidal cycle, the ratio between the upper and lower SSCs with a fixed water interval of 0.1 h was 0.77, i.e.,  $C_{1.0h} : C_{0.9h} = C_{0.9h} : C_{0.8h} = \Lambda = C_{0.2h} : C_{0.1h} = 0.77$ . Such a ratio was determined by the vertical gradient of SSCs and reflected the intensity of sediment diffusion.

As mentioned above, the linear profile can be treated as a special form of exponential profile. A similar method was used to analyze the diffusivity of the linear profile. First, the observed linear profile was fitted by the exponential function. As shown in Fig. 11, the fitted exponential profiles were very close to the measured linear profiles. Then, the diffusivity coefficient was calculated based on Eq. 5 and the fitted exponential profile. The results revealed that the diffusivity coefficient of the linear profile was also a constant value within the water column, which ranged from 0.021 to 0.058 m<sup>2</sup>/s, with the mean value of 0.030 m<sup>2</sup>/s and was notably larger than that of the exponential profile. The linear profile had the same feature as Eq. 6. For example, the linear profile appeared at the 7th hour of the ebb phase in the 14th tidal cycle, for which the ratio between the upper and lower SSCs with a water interval of 0.1 h was 0.91; i.e.,

$$C_{1.0h} : C_{0.9h} = C_{0.9h} : C_{0.8h} = \Lambda = C_{0.2h} : C_{0.1h} = 0.91$$

When the diffusivity coefficient is a constant value in the water column, the following equation can be derived from Eq. 5 (Vincent and Osborne 1995; Rose and Thorne 2001):

$$\frac{C_z}{C_a} = e^{-\frac{W_s}{\epsilon}(z-a)} \quad (7)$$

where  $C_a$  is the SSC at the height of  $a$  above the bed. Equation 7 demonstrates that the observed exponential and linear profiles were essentially the same type of SSC profile and can be expressed by a unified equation.

### Discussion: Implication of Bottom Lateral Currents in the SSC Vertical Profile and Sediment Dynamics

SSCs and salinity in the deep channel were much greater than those in the south shoal area in the North Passage due to the strong current velocity and differential advection of salinity (Shen et al. 2003; Xie 2015). The higher SSCs and salinity could be transported to the south shoal area by the bottom lateral currents, which were directed to the south flank (Fig. 2c). Thus, the SSCs in the near-bottom layer were considerably larger than that in the upper layer at the survey station, resulting in the formation of the two-layer structure SSC profile during the latter half of the flood and early half of the ebb. Simultaneously, the lower temperature water in the deep channel was also transported to the south shoal area by the bottom lateral currents. During the late flood and early ebb periods, the water temperature in the bottom layer was generally 0.5–1.5 °C lower than that in the surface layer at the survey station.

Density stratification plays an important role in estuarine sediment dynamics because it can hinder sediment diffusion and reduce the suspended sediment transport capacity (e.g., Geyer 1993; Dyer 1997; Wang 2002; Cheng et al. 2009; MacCready and Geyer 2010). Strong density stratification in the estuarine environment generally resulted from tidal straining, saltwater intrusion, and intensive resuspension (Simpson et al. 1990; Shi 2010; Wang and Wang 2010). But during this survey period, the strong density stratification was also produced by the bottom lateral currents through transporting the high-salinity and high-SSC water from the deep channel to the shoal area, leading to the gradient

Richardson numbers being significantly larger than the critical value of 0.25 at the survey station. Therefore, the bottom lateral currents were a key mechanism for the formation of the strong density stratification in the North Passage, and this may also occur in other estuaries around the world.

The bottom lateral currents also had an important influence on the suspended sediment transport rate and current-SSC correlation in the North Passage, which was mainly manifested in the following three aspects:

- (1) During the survey period, the higher near-bottom SSCs induced by the bottom lateral currents could notably enhance the landward and seaward suspended sediment transport rate and then exert an important influence on the sediment transport flux over a tidal cycle. As shown in Fig. 8, SSCs at the 3rd and 4th hours of the flood were highly related to the bottom lateral currents, which were two times of that of the 2nd hour. The high near-bottom SSCs were 65% of the total suspended sediment within the entire water column at the 3rd and 4th hours, which could notably enhance the landward sediment transport rate. During the early half of the ebb, the high near-bottom SSCs, which were induced by the bottom lateral currents, could enhance the seaward sediment transport rate. Consequently, the net sediment transport rate at the survey station was strongly affected by the bottom lateral currents.
- (2) From the 2nd to 4th hours during the flood phase (Fig. 8), with the decrease of current velocity, the SSCs increased significantly, especially for the bottom SSC. A mismatch existed between current velocity and SSC; i.e., higher SSCs occurred during the lower current period, whereas lower SSCs occurred during the higher current period (Fig. 6b). The reason for the mismatch was usually attributed to the advection of the SSC, but in this study, the mismatch should be related to the bottom lateral currents.
- (3) The high SSCs that entered the shoal area during the late flood would gradually settle onto the shoal area with the decrease of flood currents, which would further result in the siltation and geomorphological evolution of the shoal area. The rapid siltation between the dikes along the south side of the North Passage might be partly attributed to the lateral currents.

In brief, the bottom lateral currents played a prominent role in the sediment dynamics during the survey period. Specifically speaking, they can enhance the exchange of suspended sediment, salinity, and water between the deep channel and shoal area, yield strong density stratification, and exert notable influence on the SSC profiles, suspended sediment flux, and evolution of the shoal area. Lateral currents also exist in many other estuaries around the world (e.g., Lacy

and Monismith 2001; Cheng and Valle-Levinson 2009; Nidziko et al. 2009). In future research, more focus should be placed on the impact of lateral currents on the estuarine sediment dynamics.

## Conclusions

The vertical distribution of suspended sediment concentration in the TMZ of the Changjiang Estuary has been investigated using field observational data. In terms of the relationship between the SSC and the vertical stratification, the vertical profiles of SSC can be categorized into three types: (I) the two-layer structure profile, (II) the exponential profile, and (III) the linear profile. The type I mainly occurred in the conditions with high stratification, while the types II and III mainly occurred in the weak stratification and well-mixed conditions, respectively. Using the data, two new empirical expressions were derived with the aim to simulate the vertical profiles. The expressions derived in the present study were found to be accurate, simple, and easy to use, and they could be used to estimate the sediment flux given the known information of the stratification, surface and bottom sediment concentration, which can be obtained from many ways, for instance, the remote-sensed images and numerical models. The linear profile can be considered to be a special form of the exponential profile: both of them had constant diffusivity coefficients within the water column and can be expressed by a unified equation. The density stratification induced by the combination of salinity and SSC was further enhanced, which was stronger during the neap tide than during the spring tide and during the flood phase than during the ebb phase. The bottom lateral currents were directed to the south flank during most of the survey period, which could transport high-salinity, high-SSC, and low-temperature water from the deep channel to the south shoal area, resulting in strong density stratification and formation of the two-layer structure profile in the shoal area.

**Acknowledgements** Prof. Xiaohua Wang from the University of New South Wales (Canberra, Australia) and two anonymous reviewers are particularly appreciated for their constructive and helpful suggestions and comments which are fairly helpful in writing.

**Funding Information** This study is supported by the Chinese National Key Programs for Fundamental Research and Development (2016YFA0600904) and the National Natural Science Foundation of China (51761135023 and 41176069).

## References

- Cheng, P., R.E. Wilson, R.J. Chant, D.C. Fugate, and R.D. Flood. 2009. Modeling influence of stratification on lateral circulation in a stratified estuary. *Journal of Physical Oceanography* 39 (9): 2324–2337.

- Cheng, P., and A. Valle-Levinson. 2009. Influence of lateral advection on residual currents in microtidal estuaries. *Journal of Physical Oceanography* 39 (12): 3177–3190.
- Lee, G.H., C.T. Friedrichs, and C.E. Vincent. 2002. Examination of diffusion versus advection dominated sediment suspended on the inner shelf under storm and swell conditions, Duck, North Carolina. *Journal of Geophysical Research* 107 (C7): 3084. <https://doi.org/10.1029/2001JC000918>.
- Dyer, K.R. 1986. *Coastal and estuarine sediment dynamics*, 342. Chichester: John Wiley & Sons.
- Dyer, K.R. 1997. *Estuaries a physical introduction*, 195. Chichester: John Wiley & Sons.
- Fohrmann, H., J.O. Backhaus, F. Laume, and J. Rumohr. 1998. Sediments in bottom-arrested gravity plumes: numerical case studies. *Journal of Physical Oceanography* 28 (11): 2250–2274.
- Gao, S., and Y.P. Wang. 2008. Changes in material fluxes from the Changjiang River and their implications on the adjoining continental shelf ecosystem. *Continental Shelf Research* 28 (12): 1490–1500.
- Geyer, W.R. 1993. The importance of suppression of turbulence by stratification on the estuarine turbidity maximum. *Estuaries* 16 (1): 113–125.
- Grabemann, I., and G. Krause. 2001. On different time scales of suspended matter dynamics in the Weser Estuary. *Estuaries* 24 (5): 688–698.
- Hoitink, A.J.F., P. Hoekstra, and D.S. van Maren. 2003. Flow asymmetry associated with astronomical tides: implication for the residual transport of sediment. *Journal of Geophysical Research* 108 (C10): 3315. <https://doi.org/10.1029/2002JC001539>.
- Lacy, J.R., and S.G. Monismith. 2001. Secondary currents in a curved, stratified, estuarine channel. *Journal of Geophysical Research-Atmospheres* 106 (C12): 31283–31302.
- Nidzicko, N.J., J.L. Hench, and S.G. Monismith. 2009. Lateral circulation in well-mixed and stratified estuarine flows with curvature. *Journal of Physical Oceanography* 39 (39): 831–851.
- Li, Z., M.Z. Li, Z. Dai, F. Zhao, and J. Li. 2015. Intratidal and neap-spring variations of suspended sediment concentrations and sediment transport processes in the North Branch of the Changjiang Estuary. *Acta Oceanologica Sinica* 34 (1): 137–147.
- Li, Z., Y. Wang, P. Cheng, G. Zhang, and J. Li. 2016. Flood-ebb asymmetry in current velocity and suspended sediment transport in the Changjiang Estuary. *Acta Oceanologica Sinica* 35 (10): 37–47.
- Li, J.F., Q. He, W.H. Xiang, X.N. Wan, and H.T. Shen. 2001. Fluid mud transportation at water wedge in the Changjiang Estuary. *Science in China. Series B* 44 (1): 47–56.
- Liu, J.H., S.L. Yang, Q. Zhu, and J. Zhang. 2014. Controls on suspended sediment concentration profiles in the shallow and turbid Yangtze Estuary. *Continental Shelf Research* 90: 96–108.
- MacCready, P., and W.R. Geyer. 2010. Advances in estuarine physics. *Annual Review of Marine Science* 2 (1): 35–58.
- Nielsen, P. 1995. Suspended sediment concentration profiles. *Applied Mechanics Reviews* 48 (9): 564–569.
- Ogston, A.S., and R.W. Sternberg. 2002. Effect of wave breaking on sediment eddy diffusivity, suspended-sediment and longshore sediment flux profiles in the surf zone. *Continental Shelf Research* 22 (4): 633–655.
- Orton, R.M., and G.C. Kineke. 2001. Comparing calculated and observed vertical suspended-sediment distribution from a Hudson River estuary turbidity maximum. *Estuarine, Coastal and Shelf Science* 52 (3): 401–410.
- Pu, X., J.Z. Shi, G.D. Hu, and L.B. Xiong. 2015. Circulation and mixing along the North Passage in the Changjiang River estuary, China. *Journal of Marine Systems* 148 (C): 213–235.
- Rose, C.P., and P.D. Thorne. 2001. Measurements of suspended sediment transport parameters in a tidal estuary. *Continental Shelf Research* 21: 1551–1575.
- Shen, H., Z. Mao, and J. Zhu. 2003. *Saltwater intrusion in the Changjiang Estuary (in Chinese)*, 175. Beijing: China Ocean Press.
- Shen, H., and D. Pan. 2001. *Turbidity maximum in the Changjiang Estuary (in Chinese)*, 194. Beijing: China Ocean Press.
- Sheng, J., and A.E. Hay. 1995. Sediment eddy diffusivities in the near-shore zone, from multifrequency acoustic backscatter. *Continental Shelf Research* 15 (2–3): 129–147.
- Shi, J.Z., S.Y. Zhang, and L.J. Hamilton. 2006. Bottom fine sediment boundary layer and transport processes at the mouth of the Changjiang Estuary, China. *Journal of Hydrology* 327 (1–2): 276–288.
- Shi, J.Z. 2010. Tidal resuspension and transport processes of fine sediment within the river plume in the partially-mixed Changjiang River estuary, China: a personal perspective. *Geomorphology* 121 (3): 133–151.
- Shi, Z., and W.M. Chen. 2000. Fine sediment transport in turbidity maximum at the North Passage of the Changjiang Estuary (in Chinese). *Journal of Sedimentary Research* 1: 28–39.
- Shi, Z., L.F. Ren, and H.L. Lin. 1996. Vertical suspension profile in the Changjiang Estuary. *Marine Geology* 130 (1–2): 29–37.
- Shi, Z., and H.J. Zhou. 2004. Controls on effective settling speed of mud flocs in the Changjiang Estuary, China. *Hydrological Processes* 18 (15): 2877–2892.
- Simpson, J.H., J. Brown, J. Matthews, and G. Allen. 1990. Tidal straining, density currents, and stirring in the control of estuarine stratification. *Estuaries* 13 (2): 125–132.
- Song, D., and X.H. Wang. 2013. Suspended sediment transport in the Deepwater Navigation Channel, Yangtze River Estuary, China, in the dry season 2009: 2. Numerical simulations. *Journal of Geophysical Research, Oceans* 118 (10): 5568–5590. <https://doi.org/10.1002/jgrc.20411>.
- Song, D., X.H. Wang, Z. Cao, and W. Guan. 2013. Suspended sediment transport in the Deepwater Navigation Channel, Yangtze River Estuary, China, in the dry season 2009: 1. Observations over spring and neap tidal cycles. *Journal of Geophysical Research, Oceans* 118 (10): 5555–5567. <https://doi.org/10.1002/jgrc.20410>.
- Soulsby, R.L., 2000. Methods for predicting suspensions of mud. HR Wallingford Report TR 104.
- Soulsby, R.L. 1997. *Dynamics of marine sand*, 272. London: Thomas Telford.
- Thorne, P.D., A.G. Davies, and P.S. Bell. 2009. Observations and analysis of sediment diffusivity profiles over sandy rippled beds under waves. *Journal of Geophysical Research* 114 (C2): C02023. <https://doi.org/10.1029/2008JC004944>.
- Uncles, R.J. 2002. Estuarine physical processes research: some recent studies and process. *Estuarine, Coastal and Shelf Science* 55 (6): 829–856.
- Van Rijn, L.C. 2007. Unified view of sediment transport by currents and waves. II: suspended transport. *Journal of Hydraulic Engineering* 133 (6): 668–689.
- Vincent, C.E., and A. Downing. 1994. Variability of suspended sand concentrations, transport and eddy diffusivity under non-breaking waves on the shoreface. *Continental Shelf Research* 14 (2/3): 223–250.
- Vincent, C.E., and P.D. Osborne. 1995. Predicting suspended sand concentration profiles on a macro-tidal beach. *Continental Shelf Research* 15 (13): 1497–1514.
- Wang, P. 2012. Measuring and modeling suspended sediment concentration profiles in the surf zone. *Journal of Palaeogeography* 1 (2): 172–193.
- Wang, X.H. 2002. Tide-induced sediment resuspension and the bottom boundary layer in an idealized estuary with a muddy bed. *Journal of Physical Oceanography* 32 (11): 3113–3131.
- Wang, X.H., and H. Wang. 2010. Tidal straining effect on the suspended sediment transport in the Huanghe (Yellow River) estuary, China. *Ocean Dynamics* 60 (5): 1273–1283.

- Wang, Y.P., G. Voulgaris, Y. Li, Y. Yang, J. Gao, J. Chen, and S. Gao. 2013. Sediment resuspension, flocculation, and settling in a macrotidal estuary. *Journal of Geophysical Research, Oceans* 118 (10): 5591–5608. <https://doi.org/10.1002/jgrc.20340>.
- Wang, Z. 2016. *Temporal and spatial variations and transport characters of suspended sediment in the North Passage of the Yangtze Estuary (in Chinese) [dissertation]*. Shanghai: East China Normal University.
- Whitehouse, R.J.S., R.L. Soulsby, W. Roberts, and H.J. Mitchener. 2000. *Dynamics of estuarine muds: a manual for practical application*, 210. London: Thomas Telford.
- Wu, J.X., J.T. Liu, and X. Wang. 2012. Sediment trapping of turbidity maxima in the Changjiang Estuary. *Marine Geology* 303-306: 14–25.
- Xie, H. 2015. *Research on distribution characteristics of current and sediment and water-sediment flux in cross sections in the North Passage of the Yangtze Estuary (in Chinese) [dissertation]*. Shanghai: East China Normal University.
- Yang, H.F., K.H. Yang, J.D. Xu, J.D. Milliman, H. Wang, Z. Yang, Z. Chen, and C.Y. Zhang. 2018. Human impacts on sediment in the Yangtze River: a review and new perspectives. *Global and Planetary Change* 162: 8–17.
- Yang, S.L., J.D. Milliman, P. Li, and K.H. Xu. 2011. 50,000 dams later: erosion of the Yangtze River and its delta. *Global and Planetary Change* 75 (1): 14–20.